Field Analysis of a Millimeter-Wave GaAs Double-Drift IMPATT Diode in the Traveling-Wave Mode

YOSHIRO FUKUOKA, MEMBER, IEEE, AND TATSUO ITOH, FELLOW, IEEE

Abstract—**An analysis of a realistic model of distributed IMPATT structures is described. Wave equations are solved with all losses included. The results show that net gain is produced at frequencies just above the avalanche resonance, while the propagation becomes slow at high frequencies. The results compare favorably with experiment.**

I. Introduction

An IMPATT DIODE is an attractive source at millimeter-wave frequencies because it is capable of producing large power. However, as frequencies become higher, it tends to be difficult to use a sufficient device area mainly because a thinner depletion layer is required for a proper IMPATT operation. A traveling-wave structure is one way of efficiently utilizing a larger device area [1]–[4]. The electromagnetic wave traveling along the p-n junction draws some energy out of the dc current and is therefore amplified.

The most elaborate theoretical treatment of such a structure so far was done by Franz *et al.* [5]. However, their model was still too simplified because inactive layers were all assumed to be perfect conductors and the avalanche region in the depletion layer was assumed to be infinitesimally thin so that the entire depletion layer becomes a drift region. At millimeter-wave frequencies, however, the effect of the finite conductivities of these inactive regions is important. They contribute to loss and affect phase constants of the device. Also, in the active region of the device, the avalanche multiplication and the carrier drift occur simultaneously.

In the present work, a complete set of differential equations governing both wave propagation and avalanche multiplication is solved with boundary conditions, including the finite conductivities of the metal contacts. Small-signal operation is assumed, and the results are presented for a GaAs double-drift IMPATT diode. Computed gain and propagation constants are compared with experimental results published by other authors. They are qualitatively in agreement. Also, it is shown that there is an optimum thickness for each semiconductor layer, which gives maximum gain in the device.

Manuscript received May 1, 1984; revised October 10, 1984. This work was supported in part by the Joint Service Electronics Program under Grant F49620-82-0033 and in part by the U.S. Army Research Office under Contract DAAG29-81-K-0053. The manuscript was submitted for the 1984 Symposium issue, but was transferred to a regular issue due to late revision.

Y. Fukuoka is with Uniden Satellite Technology Inc., 5-13-12 Ginza, Chuo-Ku, Tokyo, 104 Japan.

T. Itoh is with the Department of Electrical Engineering, University of Texas at Austin, Austin, TX 78712.

II. Traveling-Wave IMPATT Theory

A traveling-wave IMPATT diode contains very thin semiconductor layers. Therefore, it is reasonable to assume that the field components are uniform in the transverse, horizontal direction (y-direction in Fig. 1), and a one-dimensional multilayered parallel-plate waveguide containing several semiconductor materials is a good model for the analysis of such a structure. Fig. 1 shows the side view of the double-drift traveling-wave IMPATT diode. Materials change only in the x-direction, and the electromagnetic wave is assumed to propagate in the z-direction. In the y-direction, both material constants and field components are assumed to be uniform. Under an appropriate reverse dc bias condition, the avalanche breakdown occurs mainly along the p-n junction at the center of the device. Charge carriers travel in the n and p regions at saturation velocities. A double-drift IMPATT diode is potentially capable of producing more power than a single-drift diode [6]. However, if a single-drift traveling-wave IMPATT diode is to be considered, two center regions (n and p) should be replaced with a single material. This can be considered as a special case of the double-drift device, and therefore we will develop a theory only for the double-drift device.

In a multilayered structure, the dominant propagating mode is a TM mode. This mode has only the y component of the magnetic field and the x and z components of the electric field. The analytical process is summarized as follows. A system of differential equations governing the IMPATT behavior are first solved to determine the boundary of the space-charge region. Then the wave equation is solved in each layer, including this active region, and the tangential electric and magnetic fields are matched at every boundary. The quantity obtained from the analysis is a propagation constant of the traveling wave. This is a complex quantity, and we can investigate the gain and the phase of the wave in the device.

A. Analysis of the Space-Charge Region

The space-charge region consists of the avalanche region and the drift region, in which the dc electric field is strong enough so that the carrier electrons and holes travel at

0018-9480/85/0300-0216$01.00 ©1985 IEEE

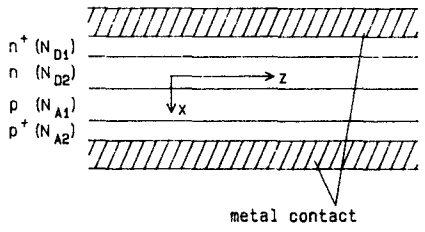

Fig. 1. Side view of a traveling-wave double-drift IMPATT diode.

saturation velocities. The carrier generation due to the avalanche multiplication occurs in the part of the space-charge region near the p-n junction where the electric field is maximum. In practice, if the p-n junction is formed by two uniform p and n materials, then the avalanche and the drift regions cannot be separated. In other words, these two processes occur simultaneously in the space-charge region. In order to physically separate these two regions, it is necessary to control the doping variation in the device (for example, Read diode [7]). In the millimeter-wave IMPATT diode, however, it is usually difficult to control the variation of the doping level in each layer near the p-n contact since the entire structure is very small. For this reason, we have to treat the space-charge region without separating it into two different regions.

The differential equations governing the IMPATT medium are as follows [5]:

$$\nabla^2\vec{E} - \nabla(\nabla\cdot\vec{E}) - \mu\epsilon\frac{\partial^2\vec{E}}{\partial t^2} - \mu\frac{\partial\vec{J}_c}{\partial t} = 0 \tag{1}$$

$$\nabla\cdot\vec{E} = \frac{q}{\varepsilon}(N_D - N_A + p - n) \tag{2}$$

$$\frac{\partial n}{\partial t} = \frac{1}{q}\left(\nabla\cdot\vec{J}_n + \alpha|J_n| + \beta|J_p|\right) \tag{3}$$

$$\frac{\partial p}{\partial t} = \frac{1}{q}\left(-\nabla\cdot\vec{J}_p + \alpha|J_n| + \beta|J_p|\right) \tag{4}$$

where

$\vec{E}$ electric field,
$\vec{J}_c$ conduction current,
$\vec{J}_n$ electron current,
$\vec{J}_p$ hole current,
N_D donor impurity concentration,
N_A acceptor impurity concentration,
n electron concentration,
p hole concentration,
α generation rate for electrons,
β generation rate for holes,
q unit charge,
ε permittivity,
μ permeability.

The first two equations are derived from the Maxwell's equations and the remaining equations represent continuity of the current and charges. Since TM mode propagation is assumed, the z component of the electric field and current densities are included in the equations. The generation rate (ionization rate) α and β are functions of the magnitude of the electric fields. We use the following relation for GaAs [8]:

$$\alpha = \beta = 3.5\times10^7 \exp\left\{-\left[\frac{6.85\times10^7}{|E(x)|}\right]^2\right\}. \tag{5}$$

To solve the differential equations (1)–(4) we have to make a few assumptions. First we separate each variable into dc and ac parts. It is assumed that the ac signal is much smaller than the dc value, and we take only the first-order sinusoidal term in the ac component (small-signal assumption). Also, we assume a traveling-wave form of the ac term which has a propagation constant γ. For example, the x component of the electric field is written as

$$E_x = E_{x\mathrm{DC}} + \tilde{E}_x e^{j\omega t - \gamma z}. \tag{6}$$

The dc bias voltage is applied only in the vertical direction (x-direction). Therefore, we retain only the x components of the dc quantities. Also, the carrier velocities in this direction is limited by the saturation velocities because of the high dc electric field in the IMPATT medium. Therefore, the relation between the x component of the current density and the carrier concentration can simply be described as

$$J_{nx} = qnv_{ns}$$
$$J_{px} = qpv_{ps} \tag{7}$$

where v_{ns} and v_{ps} are the saturation velocities of the electrons and the holes, respectively, in the semiconductor material. For simplicity, these values are assumed to be constant over the space-charge region.

Using these relations, the differential equations governing the dc components take the same form as those for a conventional IMPATT diode [9].

The differential equations for the ac components are obtained as follows:

$$\frac{d^2\tilde{E}_x}{dx^2} = \frac{1}{\varepsilon}\left(\frac{1}{v_{ps}}\frac{d\tilde{J}_{px}}{dx} - \frac{1}{v_{ns}}\frac{d\tilde{J}_{nx}}{dx}\right) + j\omega\mu\left(\tilde{J}_{nx} + \tilde{J}_{px}\right) - \left(\gamma^2 + \omega^2\mu\varepsilon\right)\tilde{E}_x \tag{8}$$

$$\frac{d\tilde{J}_{nx}}{dx} = \left[\frac{1}{v_{ns}}\left(j\omega + \frac{\sigma_n}{\varepsilon}\right) - \alpha\right]\tilde{J}_{nx} - \left(\frac{1}{v_{ps}}\frac{\sigma_n}{\varepsilon} + \beta\right)\tilde{J}_{px} - \left(J_{nx\mathrm{DC}}\alpha' + J_{px\mathrm{DC}}\beta'\right)\tilde{E}_x + \sigma_n\frac{d\tilde{E}_x}{dx} \tag{9}$$

$$\frac{d\tilde{J}_{px}}{dx} = \left[-\frac{1}{v_{ps}}\left(j\omega + \frac{\sigma_p}{\varepsilon}\right) + \beta\right]\tilde{J}_{px} + \left(\frac{1}{v_{ns}}\frac{\sigma_p}{\varepsilon} + \alpha\right)\tilde{J}_{nx} + \left(J_{nx\mathrm{DC}}\alpha' + J_{px\mathrm{DC}}\beta'\right)\tilde{E}_x + \sigma_p\frac{d\tilde{E}_x}{dx} \tag{10}$$

where α' and β' are the derivatives with respect to the electric field. Since there is no dc bias voltage applied in the z direction, we assume that the following relations between the z component of the current density and the electric field can be used:

$$\tilde{J}_{nz} = \sigma_n\tilde{E}_z$$
$$\tilde{J}_{pz} = \sigma_p\tilde{E}_z \tag{11}$$

where σ_n and σ_p are effective conductivities due to the

electrons and holes, respectively, and are assumed to be identical to the dc values

$$\sigma_n = \frac{J_{nx\mathrm{DC}}}{E_{x\mathrm{DC}}}$$
$$\sigma_p = \frac{J_{px\mathrm{DC}}}{E_{x\mathrm{DC}}} \tag{12}$$

where the high field values are used in $J_{nx\mathrm{DC}}$, $J_{px\mathrm{DC}}$, and $E_{x\mathrm{DC}}$. These are functions of space since both dc electric field and the current densities vary with respect to space position x. Actually, σ_n and σ_p should be defined by the derivatives of $J_{nx\mathrm{DC}}$ and $J_{px\mathrm{DC}}$ with respect to $E_{x\mathrm{DC}}$, rather than as stated in (12).[1] However, such a definition requires added computational effort. Further, some test calculations revealed that the numerical results reported in the latter part of the paper are relatively insensitive to the choice of σ_n and σ_p in (11).

B. Boundary Conditions

In order to solve the above differential equations, we have to specify all the boundary conditions. The boundaries of the space-charge region are not yet known and have to be determined by applying the dc boundary conditions. The dc electric field becomes almost zero outside the space-charge region since the outside regions are much more conductive compared to the space-charge region which is a depletion layer. At the space-charge region boundary in the n layer, the current consists of only electron current. Also, at the other boundary (p layer), the current consists of only hole current. By applying these conditions, we can determine the boundary on each side of the space-charge region.

Once we have found the boundaries of the space-charge region, we can apply the boundary conditions of the ac quantities. The boundary conditions on the current densities are the same as the dc case

$$\tilde{J}_{px} = 0 \qquad \text{at the boundary in n layer}$$
$$\tilde{J}_{nx} = 0 \qquad \text{at the boundary in p layer.} \tag{13}$$

We also have to match the tangential field components H_y and E_z with outside regions.

Outside of the space-charge region, we have only inactive and conductive materials. In such a region, we can write the field components as

$$H_y = A_i e^{j\xi_i x} + B_i e^{-j\xi_i x}$$
$$E_z = \frac{\xi_i}{\omega\varepsilon_i}\left(A_i e^{j\xi_i x} - B_i e^{-j\xi_i x}\right) \tag{14}$$

where

$$\xi_i^2 = \gamma^2 + \omega^2\varepsilon_i\mu$$

and A_i and B_i are constants to be determined. We can match these field components at each boundary of the metal and semiconductors, which leads to an eigenvalue equation for the propagation constant. At the space-charge region boundaries, these field quantities are transformed into field quantities used in the ac equations (8)–(10) by using the following relations:

$$\gamma H_y = j\omega\varepsilon\tilde{E}_x + \tilde{J}_{px} + \tilde{J}_{nx}$$
$$\gamma E_z = \frac{d\tilde{E}_x}{dx} - \frac{1}{\varepsilon}\left(\frac{\tilde{J}_{px}}{v_{ps}} - \frac{\tilde{J}_{nx}}{v_{ns}}\right). \tag{15}$$

The solutions of the dc and ac differential equations are obtained by the Runge–Kutta method. The second-order equation (11) is formally separated into two first-order equations, and since the ac equations are complex, they are separated into real and imaginary parts and treated as different equations. Therefore, we have a total of eight first-order coupled differential equations including dc and ac equations. In order to solve these equations numerically, the fourth- and fifth-order Runge–Kutta routine RKF45 first written by Watts *et al.* was used extensively [10]. Shooting-type iteration is then made until all the above boundary conditions are satisfied.

III. Computational Results

The parameters chosen for the numerical calculations are shown in Table I. The structure consists of eight layers and is very similar to the one used in the experiment made by Bayraktaroglu *et al.* [11]. Conductivities in the table are low-field values and used only in inactive layers. The inactive layers are treated as lossy dielectric layers and their effect is taken into account. In this diode structure, the space-charge region covers almost the entire n and p regions.

The computed results for gain and propagation constants are presented in Figs. 2 and 3, respectively. The device appears to have a loss at high frequencies because of the presence of inactive metals and semiconductors. IMPATT operation is also inefficient at these frequencies for this particular structure. As frequency decreases, the device becomes more efficient, and therefore the gain increases. Also, it is observed from Fig. 3 that the propagation becomes faster at lower frequencies. When the frequency is decreased more and approaches a certain value, the gain curve changes abruptly. The gain increases rapidly and suddenly jumps to a large loss, though it is not shown in the figure. This point is considered to be the avalanche resonance frequency, since this phenomenon is very similar to the behavior of the negative resistance of the conventional IMPATT diode [9]. Because of the abrupt change in the gain near this frequency, the device becomes unstable and the operation in this frequency range should be avoided. Therefore, the device should be used at frequencies well above this resonance frequency. In Figs. 2 and 3, dotted lines indicate the results for the special case where the depletion region is replaced by a lossless material. Slow-wave propagation becomes evident in this case. Each curve asymptotically approaches the dotted line at high frequencies.

[1] The authors are thankful to one of the reviewers who pointed out this choice.

TABLE I
PARAMETERS USED IN NUMERICAL CALCULATIONS

material	thickness (μm)	doping level (/cm³)	conductivity (S/m)
Au	7.0	——	4.3 x 10^7
Ti	0.1	——	1 8 x 10^6
n+ GaAs	0.2	5.0 x 10^{18}	6.8 x 10^5
n GaAs	0.3	1.5 x 10^{17}	2.0 x 10^4
p GaAs	0.3	1 5 x 10^{17}	9.6 x 10^2
p+ GaAs	0.2	5 0 x 10^{18}	3.2 x 10^4
Ti	0.1	——	1.8 x 10^6
Au	7.0	——	4.3 x 10^7

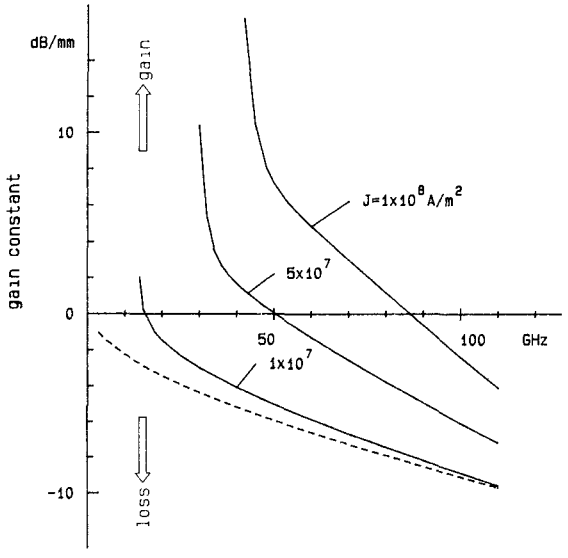

Fig. 2. Gain versus frequency: Curves are shown for three different dc current densities. ----: Active region is replaced by a lossless material.

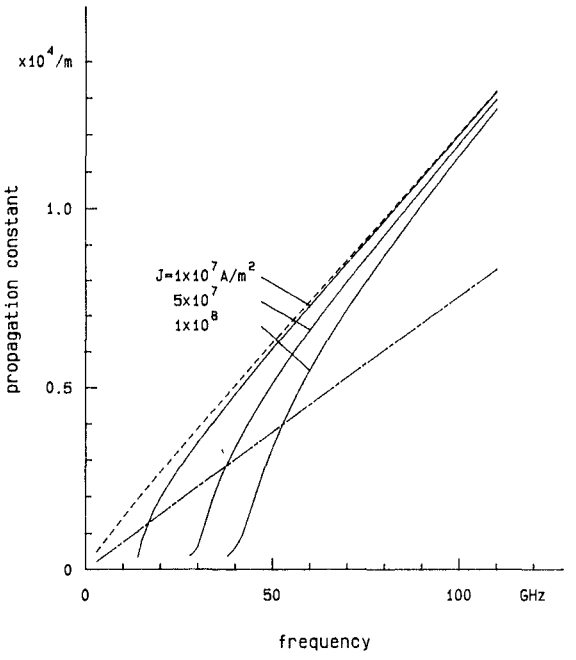

Fig. 3. Propagation constant versus frequency. ----: Active region is replaced by a lossless material. $-\cdot-\cdot\sqrt{\varepsilon_r}k_0$.

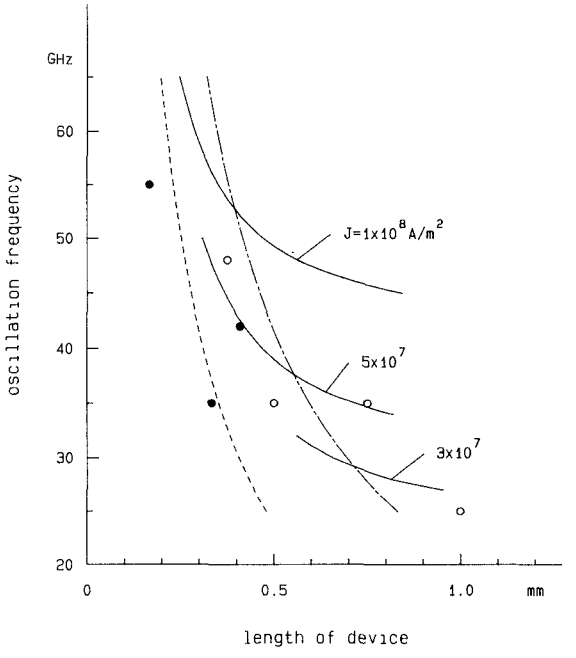

Fig. 4. Oscillation frequency versus length of device: three solid curves show theoretical results where net gain is positive. ○: experiment ($\lambda/4$) [11]. ●: experiment ($3\lambda/4$). ----: Active region is replaced by a lossless material. $-\cdot-\cdot-$: $\sqrt{\varepsilon_r}k_0$.

Fig. 4 shows a comparison of the present theory and the experimental results obtained in [11]. The device was used as an oscillator with one end open and the other shorted. In the figure, white circles (○) show the actual device lengths and the oscillation frequency obtained in the experiment, and black dots (●) show one-third of the actual device length (i.e., they are considered to be oscillating at three-quarter wavelength). The three solid curves indicate the theoretical quarter wavelength where net gain is produced in the device. They are in good agreement except for two black dots where higher order resonance ($3\lambda/4$) takes place. In these cases, the actual terminating conditions might have a more dominant effect on the oscillation frequencies.

Fig. 5 shows how gain changes with respect to the dc current. As the dc current increases, the gain also increases but suddenly goes to a large loss at a certain point. This fact qualitatively agrees with the results of power measurements for the conventional IMPATT diodes [12].

The computed field components are shown in Fig. 6. The external dc current density is set to 1×10^8 A/m^2 and frequency is 60 GHz. The device exhibits gain of about 4.8 dB/mm. The dc electric field is almost linear in both n and p regions. The avalanche multiplication occupies about 30 percent of the space-charge region near the center where the dc electron current density changes rapidly. The ac components have similar profiles. The phases of the ac electric field and the electron current density are different by more than 90 degrees where the electron current is strong (n region). The strange behavior of the phase of the

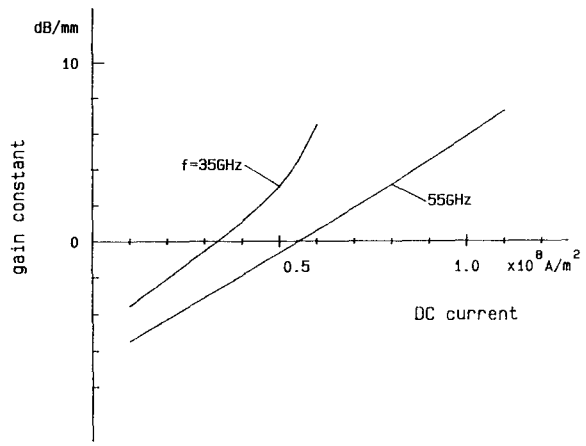

Fig. 5. Gain versus dc current.

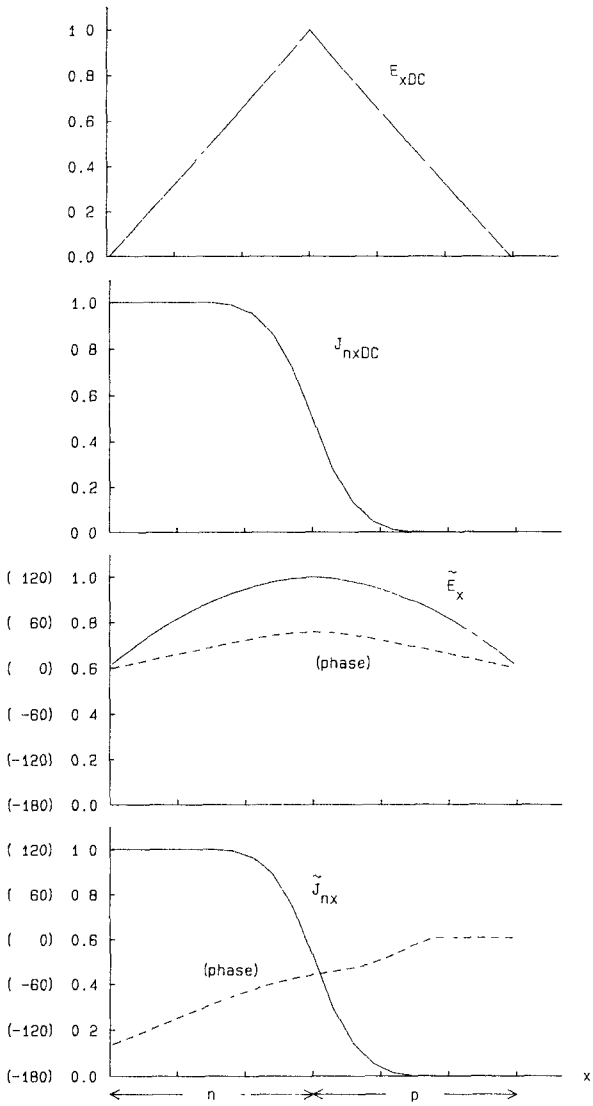

Fig. 6. Distribution of dc and ac field components: $J = 10^8$ A/m^2, $f = 60$ GHz.

ac electron current density in the p region is due to numerical error and is not important since the magnitude of the electron current is negligible.

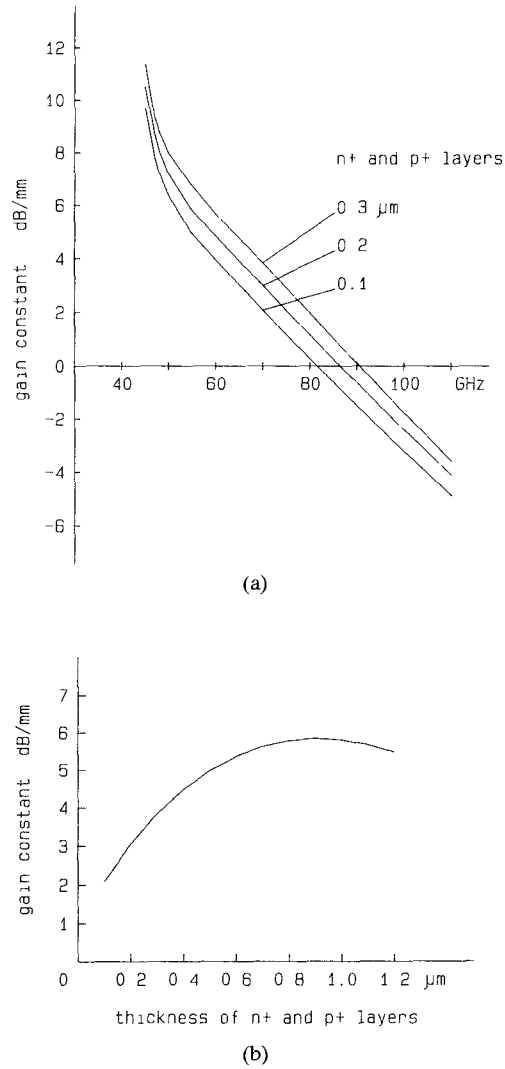

Fig. 7. Behavior of gain constant with respect to thicknesses of n^+ and p^+ layers. (a) Gain constant versus frequency. (b) Gain constant versus thicknesses of n^+ and p^+ layers: $f = 70$ GHz.

Next, we consider the device performance with respect to the dimensions of the diode. Fig. 7(a) shows the gain constant for three different thicknesses of the n^+ and p^+ layers. From this figure, the increase of the gain is observed even though larger inactive regions are added to the structure. Fig. 7(b) shows the gain constant at 70 GHz with respect to the thicknesses of the n^+ and p^+ layers. In this case, the gain constant becomes maximum value of about 5.8 dB/mm when the thicknesses are about 0.9 μm. This tendency agrees with the early prediction made by Hambleton [4].

In our calculation, we can also change the thicknesses of two inner active semiconductor layers (n and p) in order to investigate the device performance. Fig. 8(a) shows the gain constant for several different layer thicknesses. Fig. 8(b) also shows this behavior at 70 GHz. When the layer thicknesses of n and p layers are smaller than 0.3 μm, the width of the space-charge region must decrease, which results in inefficient operation. This fact is also observed

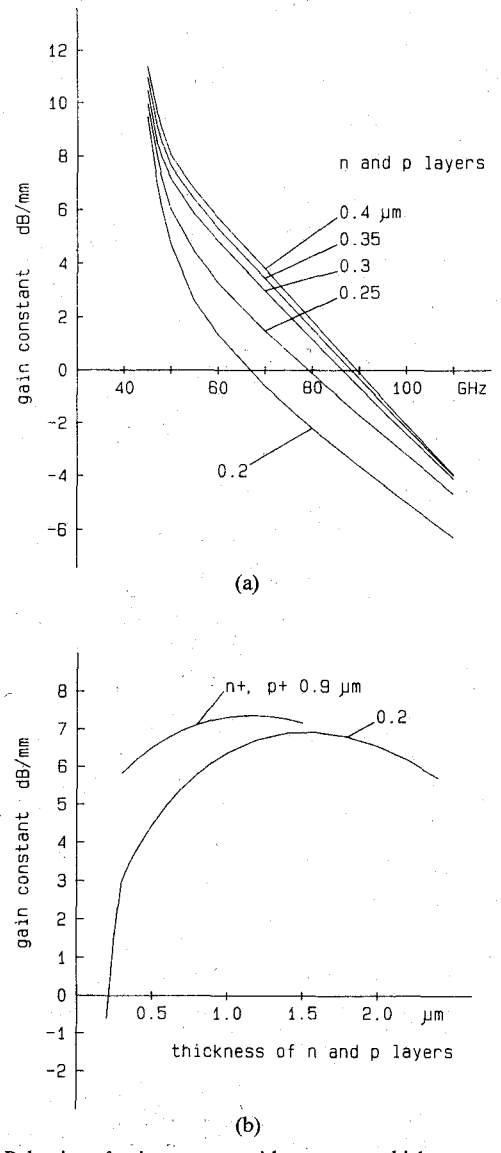

Fig. 8. Behavior of gain constant with respect to thicknesses of n and p layers. (a) Gain constant versus frequency. (b) Gain constant versus thicknesses of n and p layers: $f = 70$ GHz.

clearly from Fig. 8(b). On the other hand, if the layer thicknesses are greater than 0.3 μm, the width of the space-charge region does not change (about 0.3 μm in both n and p regions) and the excess regions only contribute as inactive layers. This has the same kind of effect as previously discussed, and we again find optimum thicknesses of about 1.5 μm, which gives maximum gain of 6.9 dB/mm (Fig. 8(b)). When the thicknesses of the n^+ and p^+ layers are increased to 0.9 μm, the optimum values reduces to 1.2 μm and the maximum gain for this value becomes 7.4 dB/mm (Fig. 8(b)).

These optimum thicknesses of the semiconductor layers are relatively large, and they should also contribute to raise the characteristic impedance level of the device, which may be advantageous for the matching to the external circuits especially when the device is used as an amplifier. However, the thick substrate often makes heat dissipation difficult and may limit the operation range of the device.

IV. Conclusion

Wave propagation phenomena in the traveling-wave IMPATT diode were analyzed numerically, and reasonable results were obtained. It was shown that the propagation was slow wave at high frequencies. As frequencies decrease and approach the avalanche resonance, the gain increases and the phase velocity becomes faster. The device performance was also investigated and it was shown that there is an optimum set of semiconductor layer thicknesses. Although it is not possible to investigate the actual behavior of the device near the avalanche resonance frequency using this method, it provides useful information of the traveling-wave IMPATT diode for normal operation range.

References

[1] M. E. Hines, "High-frequency negative-resistance circuit principles for Esaki diode applications," *Bell Syst. Tech. J.*, vol. 34, pp. 477–513, May 1960.

[2] T. A. Midford and H. C. Bowers, "A two-port IMPATT diode traveling wave amplifier," *Proc. IEEE*, pp. 1724–1725, Oct. 1968.

[3] N. S. Davydova, Yu. Z. Danyushevskiy, and L. I. Telyatnikov, "Linear theory of an IMPATT diode distributed microwave amplifier," *Telecommun. Radio Eng.*, vol. 27, no. 8, pp. 112–115, Aug. 1972.

[4] K. G. Hambleton and P. N. Robson, "Design consideration for resonant traveling wave IMPATT oscillators," *Int. J. Electron.*, vol. 35, no. 2, pp. 225–244, 1973.

[5] M. Franz and J. B. Beyer, "The traveling-wave IMPATT mode," *IEEE Trans. Microwave Theory Tech.*, vol. MTT-2, pp. 861–865, Nov. 1978.

[6] D. L. Scharfetter, W. J. Evans, and R. L. Johnston, "Double-drift-region ($p^+ pnn^+$) avalanche diode oscillators," *Proc. IEEE*, vol. 58, pp. 1131–1133, July 1970.

[7] W. T. Read, Jr., "A proposed high-frequency, negative-resistance diode," *Bell Syst. Tech. J.*, vol. 37, no. 2, pp. 401–446, Mar. 1958.

[8] S. M. Sze and G. Gibbons, "Avalanche breakdown voltages of abrupt and linearly graded p-n junctions in Ge, Si, GaAs, and GaP," *Appl. Phys. Lett.*, vol. 8, no. 5, pp. 111–113, Mar. 1966.

[9] T. Misawa, "Negative resistance in p-n junctions under avalanche breakdown conditions, Part II," *IEEE Trans. Electron Devices*, vol. ED-13, pp. 143–151, Jan. 1966.

[10] G. E. Forsythe, M. A. Malcolm, and C. B. Moler, *Computer Methods for Mathematical Computations*. Englewood Cliffs, NJ: Prentice-Hall, 1977.

[11] B. Bayraktaroglu and H. D. Smith, "Millimeter-wave GaAs distributed IMPATT diodes," *IEEE Electron Devices Lett.*, vol. EDL-4, pp. 393–395, Nov. 1983.

[12] B. Bayraktaroglu and H. D. Shih, "Integral packaging for millimeter-wave GaAs IMPATT diodes prepared by molecular beam epitaxy," *Electron. Lett.*, vol. 19, no. 9, pp. 327–328, Apr. 1983.

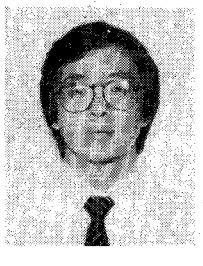

Yoshiro Fukuoka (S'81–M'84) was born in Osaka, Japan, in October 1956. He received the B.S. degree and the M.S. degree from the University of Electro-Communications in 1979 and 1981, respectively. He received the Ph.D. degree from the University of Texas at Austin in 1984. He then joined Uniden Satellite Technology in August 1984, where he is currently working on TVRO systems. His current research interests are in printed circuit components and microwave and millimeter-wave integrated circuits.

Tatsuo Itoh (S'69–M'69–SM'74–F'82) received the Ph.D. degree in electrical engineering from the University of Illinois, Urbana in 1969.

From September 1966 to April 1976, he was with the Electrical Engineering Department, University of Illinois. From April 1976 to August 1977, he was a Senior Research Engineer in the Radio Physics Laboratory, SRI International, Menlo Park, CA. From August 1977 to June 1978, he was an Associate Professor at the University of Kentucky, Lexington. In July 1978, he joined the faculty at the University of Texas at Austin, where he is now a Professor of Electrical and Computer Engineering and Director of the Electrical Engineering Research Laboratory. During the summer 1979, he was a guest researcher at AEG-Telefunken, Ulm, West Germany. Since September 1983, he has held the Hayden Head Centennial Professorship of Engineering at the University of Texas.

Dr. Itoh is a member of the Institute of Electronics and Communication Engineers of Japan, Sigma Xi, and Commission B of USNC/URSI. He serves on the Administrative Committee of IEEE Microwave Theory and Techniques Society and is the Editor of IEEE TRANSACTIONS ON MICROWAVE THEORY AND TECHNIQUES. He is a Professional Engineer registered in the State of Texas.

Coupling Parameters Between a Dielectric Resonator and a Microstripline

P. GUILLON, B. BYZERY, AND M. CHAUBET

Abstract—**The coupling coefficient between a microstripline and the dipolar magnetic ($TE_{0\gamma\delta}$) mode of a cylindrical dielectric resonator is evaluated by using two methods: numerical and analytical.**

Theoretical and experimental external quality factors, as well as the scattering matrix parameters which consider the substrate material, the ground plane, and the distance between the line and the resonator, are presented.

I. INTRODUCTION

INTEREST IN THE utilization of high dielectric constant resonators has been renewed recently because of the availability of low-loss temperature-stable materials [1], [2].

With these new technological advances in the dielectric material, practical applications of dielectric resonators in microwave devices like filters or oscillators were finally deemed feasible [3].

In a previous paper [4], we have studied the coupling between a microstripline and a dielectric resonator. The analysis uses the finite-element method to compute the magnetic field value in the dielectric resonator produced by the current flowing in the microstrip. This method gives good agreement between theoretical and experimental results, but it is not easy to use; so we propose here another similar approach, one also used in [5].

Manuscript received January 4, 1984; revised October 16, 1984. This work was supported in part by the CNES, and in part by the CNET (LANNON).

The authors are with Laboratoire de Communications Microondes et Optiques, L.A. CNRS 356, U.E.R. Sciences, 123 rue A. Thomas, 87060 Limoges, Cedex, France.

The aim of this paper is to describe two techniques for the calculation of coupling coefficient parameters which use successively the finite-difference method and an analytical one.

II. GENERAL ANALYSIS

It is well known that to couple a cylindrical dielectric resonator (permittivity ϵ_r, diameter D, height H) acting on its dipolar $TE_{0\gamma\delta}$ mode with a microstripline it is necessary to place the dielectric resonator on the plane of the substrate (permittivity ϵ_s, thickness h_s) as the magnetic lines of the resonator link those of the microstripline (Fig. 1).

A. External Quality Factor Q_e

An equivalent low-frequency network of this system [4] has been analyzed and is shown in Fig. 2. The coupling between the line and the resonator is characterized by a mutual inductance L_m. $L_r, C_r, R_r, L_1, C_1, R_L$ represent, respectively, the equivalent parameters of the resonator and of the line.

The input impedance Z_i calculated in the coupling plane is given by

$$Z_i = \frac{Z(\omega_0)}{1 + jX} \tag{1}$$

$$Z(\omega_0) = \omega_0 Q_0 \frac{L_m^2}{L_r} \tag{2}$$

$$X = \frac{2\Delta\omega}{\omega_0} \quad \text{with } \Delta\omega = \omega - \omega_0.$$

0018-9480/85/0300-0222$01.00 ©1985 IEEE